Materials & Design 227 (2023) 111800

Contents lists available at ScienceDirect

Materials & Design

journal homepage: www.elsevier.com/locate/matdes

Sensitive and responsive upconversion nanoprobes for fluorescence turn-on detection of glucose concentration

Shuai Zha [a,*], Haolan Li [b], Ga-Lai Law [c,*], Ka-Leung Wong [b,*], Angelo H. All [b,*]

[a] School of Laboratory Medicine, Hubei University of Chinese Medicine, 16 Huangjia Lake West Road, Wuhan 430065, PR China
[b] Department of Chemistry, Hong Kong Baptist University, 224 Waterloo Road, Kowloon, Hong Kong
[c] Department of Applied Biology and Chemical Technology, The Hong Kong Polytechnic University, Hong Hum, Kowloon, Hong Kong

HIGHLIGHTS

- Ultrasensitive and rapid detection strategy of glucose was constructed based on lanthanide-doped upconversion nanoprobe.
- The functionalized nanoprobe can distinguish cancer cells from normal cells by *in vitro* emission intensity via optical bioimaging.
- The designed nanoprobe would facilely achieve glucose detection in situ and *in vitro* with ultralow detection limit.

GRAPHICAL ABSTRACT

We developed the functionalized upconversion nanoprobe with ultrasensitive and responsive properties for glucose detection, the responsive emission and satisfactory differentiated performances are observed *in situ* and *in vitro*.

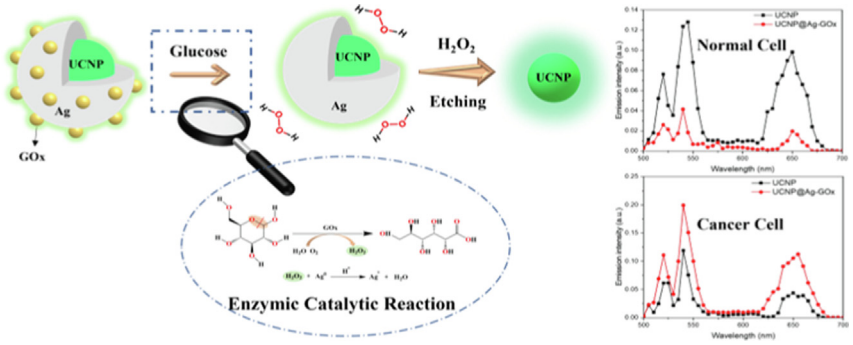

ARTICLE INFO

Article history:
Received 22 December 2022
Revised 5 February 2023
Accepted 26 February 2023
Available online 28 February 2023

Keywords:
Lanthanide-doped upconversion nanoparticles
Optical bioimaging
Surface modification
Glucose detection
Upconversion emission recovery

ABSTRACT

Various approaches for detecting glucose concentration in real time are emerging at a breakneck pace. Glucose metabolism is closely linked to severe pathological events, which would either cause or predispose many progressive diseases in human. Herein, hydrophilic upconversion nanoprobes $NaGdF_4$: Yb^{3+}, Er^{3+}@Ag anchored with glucose oxidase (GOx) for glucose detection with lower detection limits have been efficaciously constructed. In the upconversion nanoprobes, $NaGdF_4$: Yb^{3+}, Er^{3+} cores, and Ag layers act as energy donors and effective quenchers, respectively, through energy transfer. Moreover, the layer of Ag may disintegrate by H_2O_2 in the presence of glucose when glucose oxidase anchoring on the exterior of $NaGdF_4$: Yb^{3+}, Er^{3+}@Ag nanoprobes, which leads to the phenomenon of upconverting emission recovery. Additionally, $NaGdF_4$: Yb^{3+}, Er^{3+}@Ag-GOx has an ultralow detection limit of 1.77 μmol L^{-1} on glucose detection, and it can achieve optical bioimaging to distinguish cancer cells from normal cells. As a result, the $NaGdF_4$: Yb^{3+}, Er^{3+}@Ag nanoprobes could be expanded to detect diverse H_2O_2-involved analytes. Overall, this nanoprobe has promising potential to be a compelling tool for the biomedical applications.

* Corresponding authors.
E-mail addresses: shuaizha1@hbtcm.edu.cn (S. Zha), ga-lai.law@polyu.edu.hk (G.-L. Law), klwong@hkbu.edu.hk (K.-L. Wong), angelo@hkbu.edu.hk (A.H. All).

https://doi.org/10.1016/j.matdes.2023.111800
0264-1275/

1. Introduction

Glucose is a vital bioactive molecule that is indispensable for human body metabolisms and functions, though it also has a significant impact on human health. High blood pressure, heart diseases, impaired vision, renal failure, diabetes, and other metabolic illnesses can be linked to either excess or deficit of blood glucose (so-called high and low glycemia) [1–5]. Cancer cells have been shown to undergo typical changes in their metabolic processes, such as enhanced glucose uptake, increased rates of glutaminolysis, and fatty acid synthesis, indicating that these shifts promote the proliferation and survival of tumor cells. Considering the pivotal role of glucose in maintaining healthy body functions, evidently, detecting glucose concentration with utmost accuracy, sensitivity, and specificity screening is crucial, particularly for an early diagnosis of various diseases.

To date, most glucose concentration measurement methods have centered on electrochemical, colorimetric, and fluorescence techniques [6–13]. Nevertheless, the majority of these techniques have critical limitations. For instance, they require complex equipment, have intricate experimental procedures, and mostly are time-consuming sample immobilization treatments. As a matter of fact, although small organic fluorescent agents have vast biomedical applications [14–19], lanthanide-based upconversion nanocrystals have better chemical and photophysical features than organic fluorescent dyes and quantum dots, including minimal toxicity, significant Stokes shifts, narrow emission peaks, extended emission lifetimes, and strong photobleaching resistance [20,21]. In theory, upconversion is the process that efficiently converts low-energy excitation photons, which are normally near-infrared (NIR) light, into higher energy output (e.g., NIR, visible, ultraviolet) through the practice of long lifetime and authentic ladder-like energy levels of trivalent lanthanide ions embedded in the lattice of the desired inorganic host. As a result, the wavelength of excitation is longer than the emission wavelength. In other words, the upconversion processes of nanoparticles commonly absorb two or more lower energy photons to emit one higher energy photon. Furthermore, upconversion nanomaterials (UCNMs) doped with lanthanide ions feature ladder-like energy levels which can emit emissions ranging from ultra-violet to visible wavelengths under particular excitation wavelengths. More importantly, lanthanide-based UCNMs have a number of benefits over typical fluorescent probes (such as organic fluorescent dyes, metal compounds, or inorganic quantum dots) [22]. These unique benefits include (but are not limited to): non-autofluorescence, high chemical stability, deep light penetration, extended lifetime, limited sample damage, and minimal biotoxicity. Therefore, UCNMs have significant prospects in biomedical applications, such as *in vivo* bioimaging, biosensing, and nanomedicine [23–31].

In fact, some highly designed specific function-engineered UCNM-based probes have widely been employed in the detection of glucose. MnO_2 nanosheet-modified upconversion nanoparticles were designed by Chu et al. for glucose detection in human serum and blood samples, which was achieved via H_2O_2 modulation of MnO_2-induced upconverted luminescence quenching of UCNPs with detection limit 3.7 μM [32]. Additionally, DNA-AgNPs based on upconversion nanoparticles were developed later for the sensing of H_2O_2 and glucose by luminescence resonance energy transfer. The low limit of detection 2.65 μM was estimated in the solution [33]. In another study, the squaric acid (SQA)-iron (III) linked with upconversion nanoparticles for the highly sensitive detection of glucose levels in human serum via the inner filter effect was synthesized by Yao et al. [34]. However, none of them can achieve glucose detection *in vitro* through non-invasive means - optical bioimaging.

Optical bioimaging refers to the use of optical detection methods combined with fluorescent probes to image cells or tissues or even organisms to obtain biological information. Importantly, optical bioimaging has the advantages of mature detection instruments, high sensitivity, high contrast, high resolution, intuitive imaging, good trackability, fast imaging speed, and non-destructive detection, which have been widely utilized in various biological applications [35–37], for instance, intracellular ions detection [38], cellular localization [39] and imaging-guided therapy [40]. However, there are rare reports on upconversion-based glucose detection at the cellular level by *in vitro* emission intensity measurement.

Herein, we report an upconverting fluorescence approach for expeditious detection of glucose concentration by employing $NaGdF_4$:Yb^{3+}, Er^{3+}@Ag core–shell nanoparticles. After anchoring of glucose oxidase (GOx) on the exterior of the core–shell nanoparticles, the fluorescence of $NaGdF_4$:Yb^{3+}, Er^{3+} (UCNP) can be restored by adding glucose, which is capable of oxidizing the Ag layers to Ag^+ owing to the generation of H_2O_2 via glucose enzymatic conversion induced by GOx. It is intriguing to underline that the design strategy for the detection technique of glucose concentration is based on the upconversion emission recovery of UCNP@Ag-GOx nanoprobe upon the presence of H_2O_2. This specific design allows for one-pot detection of glucose concentration, where multiple-step reactions can proceed with cascade. Additionally, the exceptional discriminatory photophysical property has been verified among interfering substances, in which the limit of detection of the nanoprobe is calculated to be 1.77 μmol L^{-1}. In fact, the uniqueness and inspiration of this work are that distinguishes cancer cells from normal cells via optical bioimaging and compare directly through *in vitro* emission intensity. There is a 5-fold emission intensity difference between HeLa cancer cells and MRC-5 normal cells. Additionally, the functionalized and facile-synthesized nanoprobes with the efficient energy transfer pair of Yb-Er possess the characteristics of deep penetration, minimized light damage to cells and zero-autofluorescence due to its excitation at 980 nm. Because the emission of the nanoprobe locates in the visible range, it is intuitive to discriminate cancer cells from normal cells by the indication of *in vitro* emission intensity and the naked eye under a fluorescent microscope. Hence, the convincing results strongly confirm that this novel nanoprobe has promising potential to detect biomarkers in the biomedical research that could be further exploited for theranostics applications.

2. Materials and methods

2.1. Materials

Rare-earth acetates $Gd(CH_3CO_2)_3{\cdot}4H_2O$ (99.9% trace metals basis), $Yb(CH_3CO_2)_3{\cdot}4H_2O$ (99.9% trace metals basis), and $Er(CH_3CO_2)_3{\cdot}4H_2O$ (99.9% trace metals basis), ammonium fluoride (99 %), cyclohexane (99.5 %), ethanol (99.7 %), hydrochloric acid, methanol, oleic acid (90 %), 1-octadecene (90 %), sodium hydroxide (99 %), silver nitrate, glucose, bovine serum albumin, human serum albumin, fructose, sucrose, lysine and glycine were purchased from Sigma–Aldrich. Trisodium citrate, glutaraldehyde and spermine were provided by Energy Chemical (Anhui Province, China). Glucose oxidases (100 U/mg) were offered by Macklin (Shanghai, China) and GOx were preserved at 4 ℃ for long-term storage. Deionized water was used to form metal salt solutions, while methanol was utilized to prepare NH_4F and NaOH solutions. All the chemicals and reagents were used without purification. Ultrapure H_2O was obtained from Millipore Milli-Q direct water purification system.

2.2. Synthesis of Water-soluble UCNP

The UCNPs were prepared similarly following our previously reported approach via the coprecipitation method [23]. In a typical experiment, 4 mL of an aqueous solution including $Gd(CH_3CO_2)_3 \cdot 4H_2O$, $Yb(CH_3CO_2)_3 \cdot 4H_2O$, $Er(CH_3CO_2)_3 \cdot 4H_2O$, 6 mL of oleic acid and 15 mL of 1-octadecene were dropped, mixed, and stirred in the 50 mL three-neck round-bottom flask. The admixture was heated to 150 ℃ for 20 min and then maintained at room temperature for 30 min. After that, NH_4F and NaOH solutions (5 mL) were slowly added into the above mixed solutions, then stirred for 30 min. The reaction temperature was kept at 150 ℃ under a vacuum environment, followed by rising the temperature to 300 ℃ for 1.5 h with nitrogen flow. Then, the mixture solution was cooled down to room temperature, and the product was washed with cyclohexane and ethanol solutions (volume ratio 1:2) three times and collected via centrifugation. Finally, the precipitated product with light yellow dispersed in cyclohexane was treated with 1 M hydrochloric acid for 1 h with sonication at 45 ℃ to remove the oleic acid on the surface of nanoparticles, followed by high-speed centrifugation at 14100 rpm four times. After discarding the supernatant, the hydrophilic UCNP, which has a milk-like color, was dispersed in a trisodium citrate solution at 4 ℃ for further use.

2.3. Preparation of UCNP@Ag

The UCNP trisodium citrate solution (∼5 mg/mL) obtained from the last step and silver nitrate solution (5 mL) were evenly mixed in a round-bottom flask and stirred (∼500 rpm) at room temperature for 1 h. Afterward, the mixture solution was heated to 100 ℃ gradually and maintained the condition overnight with vigorous stirring. The precipitated UCNP@Ag was rinsed with deionized water and centrifuged at 14100 rpm three times (30 min each time). Further, UCNP@Ag was dried under compressed air at room temperature.

2.4. Immobilization of GOx on UCNP@Ag

The UCNP@Ag that we obtained from previous processes was transferred to 5 mL of 3 wt% glutaraldehyde solution in a flask. The solution was desiccated at room temperature after vigorous stirring. Subsequently, 15 mL of GOx solution (100 U mg^{-1}) was employed to anchor GOx on the surface of UCNP@Ag at 4 ℃ for 36 h. After that, the final product was rinsed with double-distilled H_2O and centrifuged (14,100 rpm, 30 min) three times before being ultrasonically dispersed in 10 mL ultrapure H_2O. UCNP@Ag-GOx solutions were stored at 4 ℃ for later use.

2.5. Glucose detection

1 mL UCNP@Ag-GOx solutions were prepared at the concentration of 5 mg/mL, followed by adding glucose solution at various concentrations and diverse interfering chemicals (spermine, lysine, glycine, bovine serum albumin, human serum albumin, fructose, sucrose, and various metal ions). After that, the solution was diluted to 2 mL with ultrapure H_2O before being completely mixed. The fluorescence spectra of the mixed solution were monitored after a 1-minute incubation at room temperature. The signal data were recorded and saved in HORIBA software for later treatment.

2.6. Characterization assays

The equipment was utilized to analyze and characterize the as-prepared nanoprobes such as transmission electron microscopy (TEM), X-ray powder diffraction (XRD) diffractometer, Fourier transform infrared (FTIR) spectrometer, and dynamic light scattering (DLS) analyzer. Specifically, 1 mL of UCNP and UCNP@Ag-GOx (∼1 mg/mL) solutions were added in the eppendorf tubes with ultrasound for 30 min, then UCNP and UCNP@Ag-GOx dissolved in ultrapure H_2O were taken and dropped in carbon-coated copper grids. After drying at room temperature overnight, the grids were observed under TEM at 100 kV. Then, the TEM images of UCNP and UCNP@Ag-GOx were obtained and stored. The powder forms (∼5 mg) of UCNP and UCNP@Ag-GOx were prepared through freeze-drying means and utilized to test XRD patterns via Bruker AXS D8 Advance X-ray diffractometer. After that, the powders of the as-synthesized samples were placed on the surface of the sample area in the FTIR spectrometer, and the FTIR spectra of UCNP and UCNP@Ag-GOx were measured by Fourier Transform Infrared Spectrometer (Perkin Elmer FTIR Spectrum II) at room temperature (detection range: 400–4000 cm^{-1}). Subsequently, the signals of scattered light induced by the Brownian motion of the nanoparticles were recorded upon laser irradiation in a Beckman DelsaMax Core light scattering analyzer, and then the DLS size and size distributions of UCNP and UCNP@Ag-GOx were collected by the DLS analyzer under optimal parameter settings. Thereafter, the visible emission spectra of UCNP and UCNP@Ag-GOx were measured by SpectroFluorometer System (Horiba/Fluoromax-4) at room temperature. In general, the nanoprobes was sonicated for well-dispersed purpose before adding into the quartz cuvette (maximum capacity: 3.5 mL, 10 mm light path) in the sample holder, then the detection range of the machine was set as 500–700 nm upon external 980 nm laser excitation source with 1.6 mW power (Beijing Laserwave Optoelectronics Technology Co., Ltd). All the data was compiled and analyzed using Origin software.

2.7. Cell culture

The HeLa and MRC-5 cells were cultured in T25 cell culture flask with Dulbecco's Modified Eagle Medium (DMEM) (Gibco) and minimum essential medium (MEM) supplemented with 10% FBS (Gibco) and antibiotics (penicillin, 50 μg mL^{-1}; streptomycin, 50 μg mL^{-1}), respectively. HeLa and MRC-5 cells were incubated at 37 ℃ in a standard incubator with 5% CO_2 flow.

2.8. In vitro confocal imaging

The HeLa and MRC-5 cells were washed with PBS three times after 24-hour incubation with UCNP and UCNP@Ag-GOx. The images were obtained by a confocal laser scanning microscope, Leica TCS SP8, equipped with a Ti: Sapphire laser. The operation excitation wavelength is 980 nm (power = 0.89 mW), and the detection range is 500–700 nm.

3. Results and discussions

3.1. Preparation and characterizations of the nanoprobes

The hydrophilic nanoprobes were constructed via facile synthesis approaches and the strategy for fluorescence turn-on detection of glucose concentration was displayed in Scheme 1. Firstly, the TEM view of the UCNP in Fig. 1A reveals that the as-prepared UCNP is well-dispersed, with an average size of 21 nm. The high-resolution TEM (HRTEM) image of the UCNP@Ag-GOx nanoprobes is shown in Fig. 1B. A thin Ag layer can be found on the exterior of UCNP (indicated by the red arrow), which would increase the size of UCNP@Ag-GOx to roughly 25 nm. The homogeneous morphology of the UCNP@Ag-GOx is remarkably similar to the UCNP parents. According to our TEM results, the thin layer of Ag coated on the surface of the UCNPs is well-observable, and the nanoprobes are clearly monodisperse in an aqueous solution. Ag shells are

observed at the periphery of UCNPs. The overall architectures are regarded as intact nanostructures, which indicates the successful conjugation of UCNP with Ag shells. Moreover, the XRD spectra of UCNP and UCNP@Ag-GOx are shown in Fig. S1, Supporting Information. The XRD patterns of bare UCNP (green line) and UCNP@Ag-GOx (blue line) exhibit their highly crystalline form, with all diffraction peaks matching well with these standard hexagonal phase structures of $NaGdF_4$ (ICDD#27-0699). The FTIR transmission spectrum was further utilized and recorded to pinpoint the structures of UCNP and UCNP@Ag-GOx. The C–H bond's stretching vibrations (Fig. S2) displayed absorption peaks at 2920 and 2851 cm^{-1}, which are the typical peaks of the UCNP [21]. Hence, XRD patterns and FTIR spectra suggest no additional impurity peaks identified during surface modification and no impurity generated during the synthetic process, respectively. Additionally, zeta-potential measurement and energy-dispersive X-ray spectroscopy (EDS) analysis were further performed to evidence surface charge changes and the element analysis in the nanoprobes, respectively. Fig. S3 showed the zeta potential of ligand-free (LGF)-UCNPs were initially measured as 19.23 mV, then the values of UCNP@Ag and UCNP@Ag-GOx were recorded as 6.96 mV and 9.68 mV respectively due to the successful coating of Ag NPs (negative charge) and GOx. The EDS analysis has been measured in Fig. S4. From the EDS patterns, it could be seen that Ag, Na, Gd, F, Er, and Yb were present in the as-prepared UCNP@Ag-GOx nanoprobe after surface modification, which was evidenced that Ag NPs were adsorbed on the surface of UCNP. These demonstrate the successful surface modification during the synthesis process of UCNP@Ag-GOx. Additionally, inductively coupled plasma mass spectrometry (ICP-MS) was applied for examining the amount of Ag in the as-developed samples. As shown in Fig. S5, ICP-MS measurement for Ag amount in UCNP, UCNP@Ag, and UCNP@Ag-GOx was conducted after storing for 1 day and 7 days respectively. Obviously, the presence of Ag in UCNP@Ag and UCNP@Ag-GOx was observed, which implied the successful conjugation among UCNP, Ag, and GOx.

Furthermore, to test the stability of the as-prepared samples, DLS measurements are generally conducted to verify the aggregation extent of the as-synthesized products. The solutions of UCNP and UCNP@Ag-GOx displayed ignorable aggregation in ultrapure H_2O and phosphate buffer solution (PBS) after 1 day and 7 days, as shown in Fig. 1C and D. Furthermore, the size distributions and DLS sizes of the as-prepared samples are almost same as samples' after the storage for 7 days. This indicates that the as-synthesized nanoprobes possess the excellent dispersibility and stability in physiological solutions. Moreover, DLS measurements corroborate that the upconversion nanoprobe possesses high stability, little aggregation tendency, and uniform size distribution, which are exceptionally consistent with the TEM images.

3.2. Photophysical properties study

The emission spectra of UCNP@Ag-GOx with varying Ag concentrations are shown in Fig. 2A. The emission intensities of UCNP@Ag-GOx showed steadily decline along with the increase of Ag concentration, which suggested that the upconversion emission of UCNP is obviously quenched by Ag layers through energy transfer from the UCNP to Ag. Characteristically, the energy levels of the states between Yb^{3+} and Er^{3+} are rather near, allowing for efficient energy transfer. Following that, an extra energy transfer from another Yb^{3+} to the Er^{3+} happens, resulting in further Er^{3+} excitation ($^4F_{7/2}$). The doubly exited Er^{3+} produces one photon (~520, 540, or 653 nm, respectively), whose energy is marginally less than that of two 980 nm photons after rapid nonradiative relaxation to one of three lower-energy states ($^2H_{11/2}$, $^4S_{3/2}$, or $^4F_{9/2}$) (Scheme S1).

Additionally, the following transitions correlate to the emission peaks: $^2H_{11/2} \rightarrow {}^4I_{15/2}$ (~520 nm), $^4S_{3/2} \rightarrow {}^4I_{15/2}$ (~540 nm), and $^4F_{9/2} \rightarrow {}^4I_{15/2}$ (~653 nm), which suggest the efficient energy transfer between the doping lanthanide ions (Yb^{3+} and Er^{3+}) in UCNP. Furthermore, Fig. 2B exhibits the effect of Ag doping concentration on the quenching effectiveness of UCNP@Ag-GOx at 540 nm. The quenching efficiency is determined as $(F_0\text{-}F)/F_0$, where F_0 and F are the intensities of emission at 540 nm in the absence of and presence of the Ag layer, respectively. The maximum doping concentration of Ag in UCNP@Ag-GOx (Ln^{3+}: Ag^+ = 1: 0.25) is corresponding to the largest quenching efficiency (~85%). The fluorescence intensity of UCNP without Ag doping is almost 7-fold greater than that of UCNP coating on the highest concentration of Ag due to the Ag shell coating, which leads to the drastic fall of the emission.

3.3. Selectivity studies

It is significant to determine the capacity of probes to distinguish the target from interfering molecules and showcase specific responses to the target. Therefore, the visible response emission spectra of UCNP@Ag-GOx were investigated to verify the selectivity of the nanoprobe in the presence of various interfering species, including proteins, saccharides, amino acids, and metal ions, as displayed in Fig. 3. The relative upconversion fluorescence response is calculated and presented as $(f\text{-}f_B)/f_B$, where f and f_B are the emission intensities at 540 nm with and without analytes, respectively. Furthermore, UCNP@Ag-GOx shows (i) negligible emission

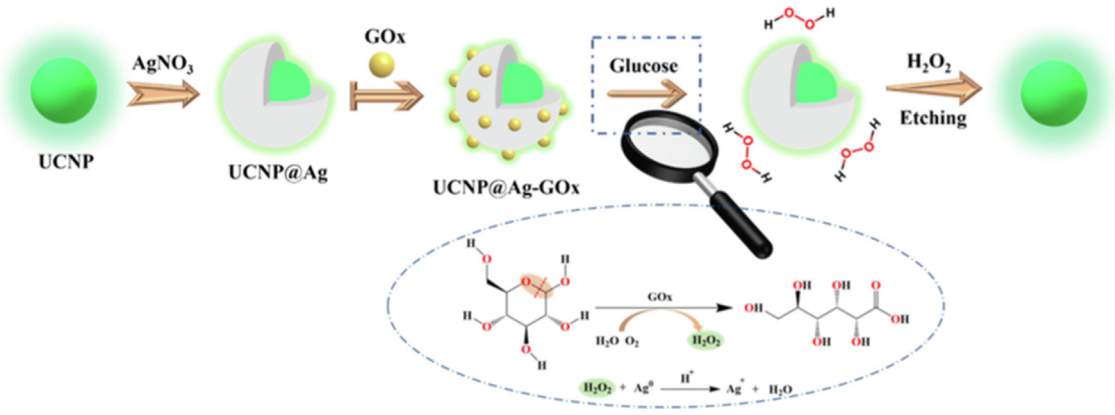

Scheme 1. Schematic illustration on design and mechanism of UCNP@Ag-GOx for glucose concentration detection.

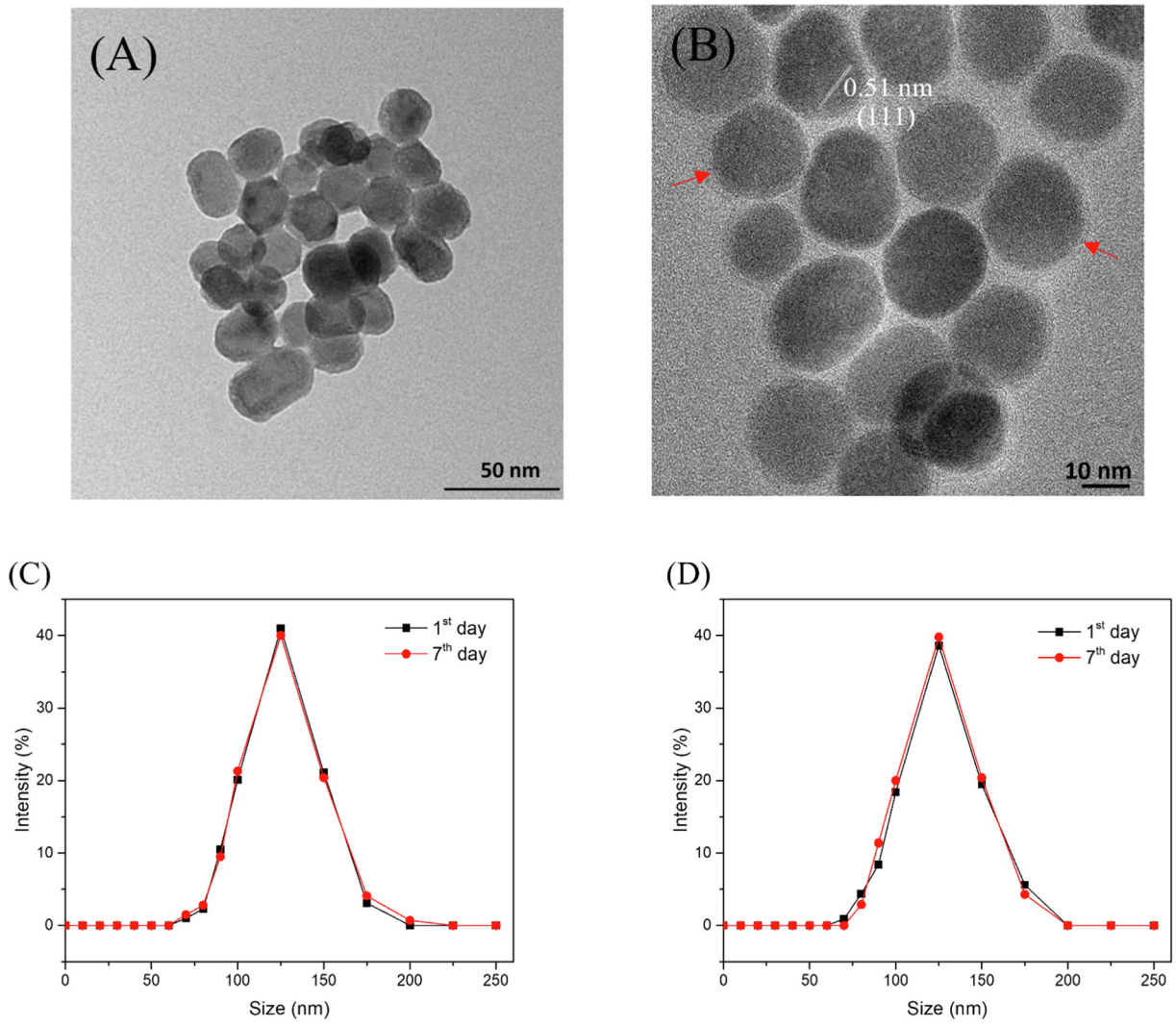

Fig. 1. (A) TEM images of UCNP (scale bar: 50 nm). (B) HRTEM image of UCNP@Ag-GOx (scale bar: 10 nm). DLS measurements and stability studies of UCNP@Ag-GOx (C) in H_2O (D) in PBS.

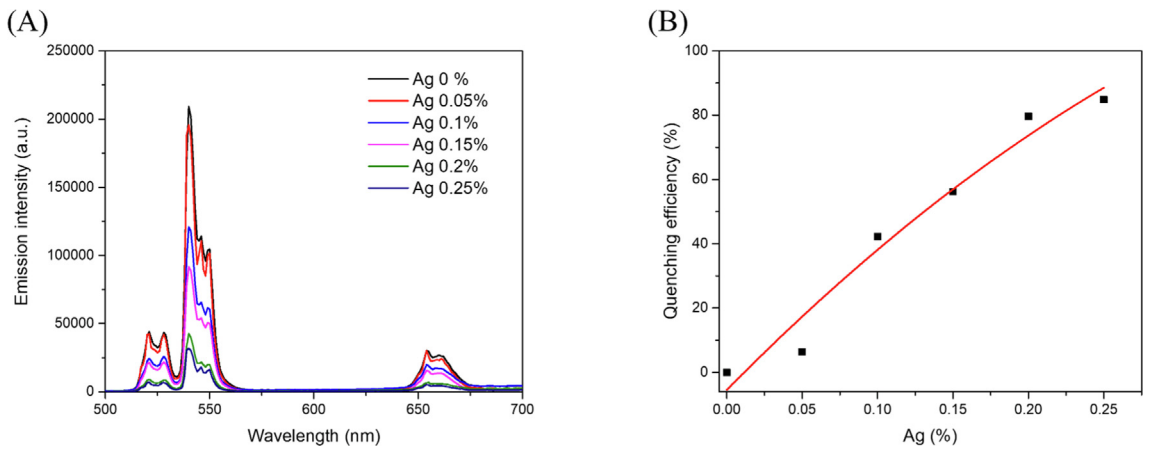

Fig. 2. (A) Emission spectra of UCNP@Ag-GOx with various Ag concentrations. (B) Relationship between the emission quenching efficiency of UCNP@Ag-GOx at 540 nm and the Ag concentrations.

changes under 5 μM of abundant metal ions, (ii) modest emission response among the 5 μM addition of bovine serum albumin (BSA), human serum albumin (HSA), fructose, sucrose, and (iii) strong fluorescence response for the incubation with 5 μM glucose. Further, it is known that the nanoprobes are exceptionally more selective to conduct the detection of glucose concentration compared to the spermine, lysine, glycine, BSA, HSA, fructose, sucrose, and various metal ions. Additionally, our nanoprobes are capable of displaying

specific and sensitive elevated emission responses toward the changes in the glucose concentration from selectivity investigations (Fig. 3A).

In addition, we hope to apply this method for practical application in physiological conditions and test the selective and responsive capability of the nanoprobe in simulated physiological conditions, so the interferences of BSA, HSA, Ca^{2+}, and Na^{+} are carried out in glucose solution in the selectivity study. As shown in Fig. 3B, only glucose can lead to drastic and substantial upconversion emission recovery from quenching, while other substances

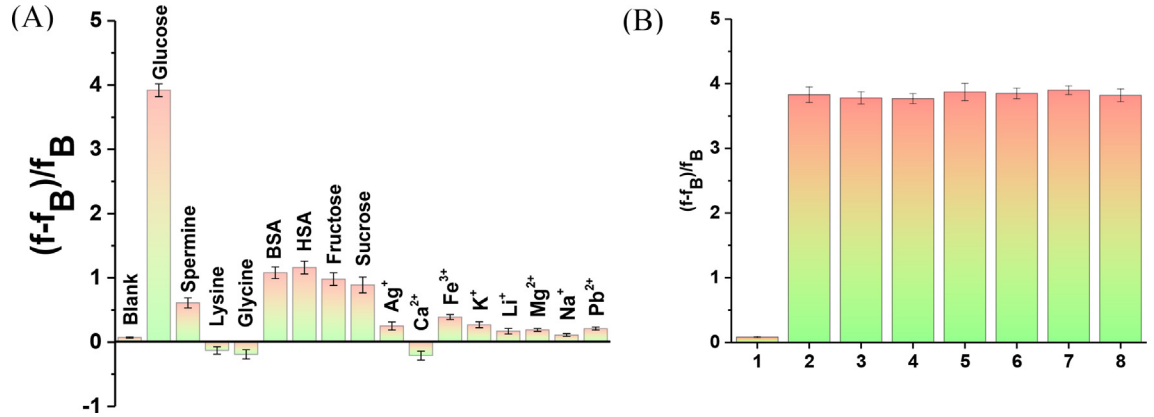

Fig. 3. (A) Visible emission ratio of UCNP@Ag-GOx (1 mg mL^{-1}, λ_{ex}: 980 nm) in H_2O among various analytes at 540 nm. (B) Interference study in simulated physiological conditions. Labels from left to right are 1: blank, 2: 5 μM glucose solution, 3: 50 μM BSA in 5 μM glucose solution, 4: 50 μM HSA in 5 μM glucose solution, 5: 50 μM Na^{+} in 5 μM glucose solution, 6: 50 μM Ca^{2+} in 5 μM glucose solution, 7: 150 mM NaCl in 5 μM glucose solution, 8: 0.9 % saline solution in 5 μM glucose solution.

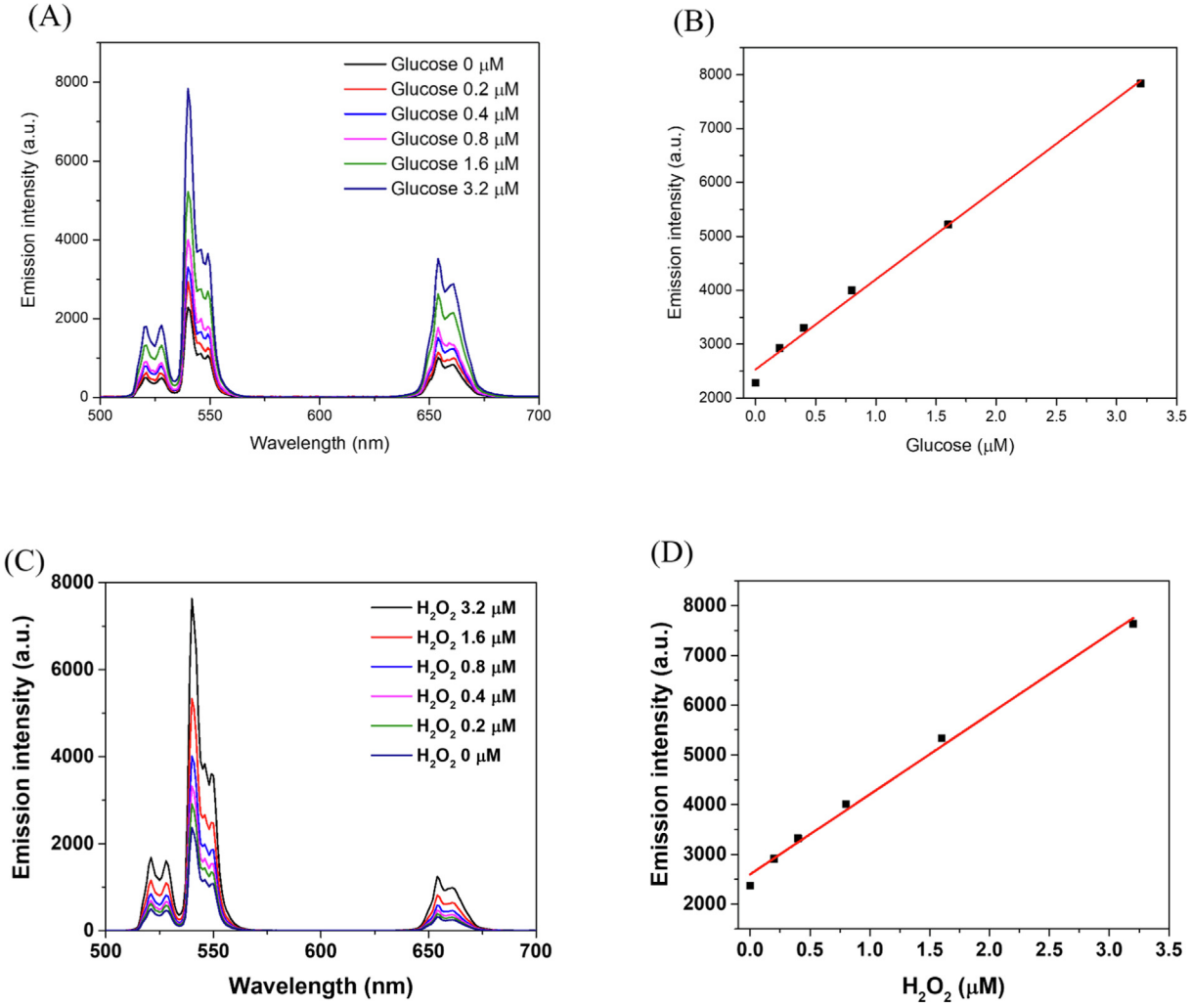

Fig. 4. (A) Emission spectra of UCNP@Ag-GOx along with the diverse concentration of glucose in H_2O. (B) The plot of the emission intensity at 540 nm over the glucose concentration. (C) Emission spectra of UCNP@Ag with the addition of H_2O_2. (D) The plot of the emission intensity at 540 nm over the H_2O_2 concentration.

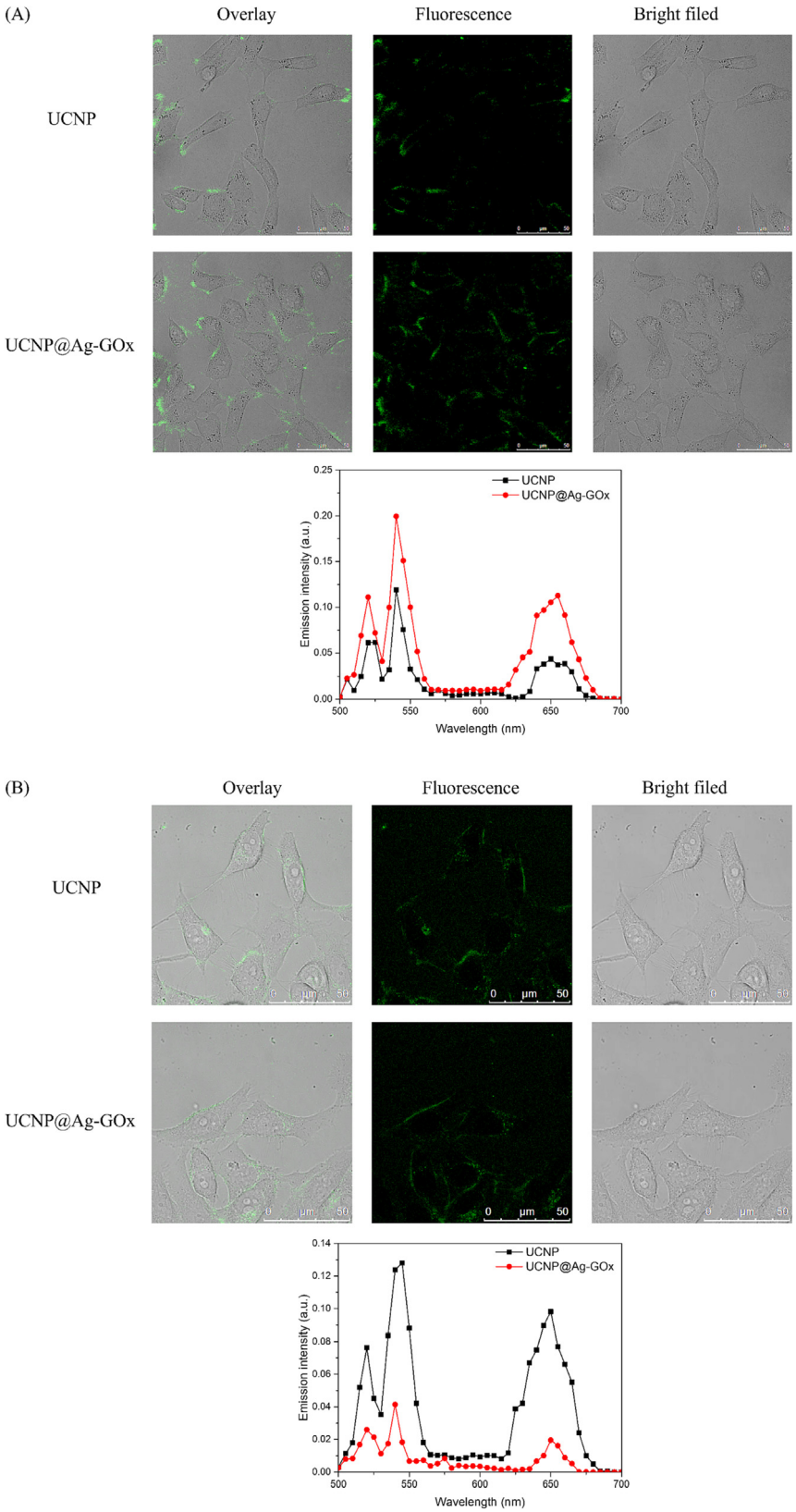

Fig. 5. In vitro confocal imaging and *in vitro* emission spectra of UCNP and UCNP@Ag-GOx in (A) HeLa cells and (B) MRC-5 cells. (λ_{ex}: 980 nm, λ_{em}: 500–700 nm).

hardly influence the emission intensity in the presence of glucose, even though their concentration is ten times that of glucose. To further examine the selectivity performance and mimic physiological conditions, the interferences of the 150 mM NaCl and 0.9 % saline solution are also conducted in glucose solution. Consequently, negligible changes are observed. Therefore, this method can act as a highly selective and useful sensing strategy for the detection of glucose.

3.4. Detection of glucose

Given the critical significance of glucose concentration monitoring, the potential of using UCNP@Ag-GOx nanoprobe for glucose concentration detection is further investigated. UCNP@Ag-GOx (Ln^{3+}: Ag^{+} = 1: 0.1) is employed to detect glucose concentration. Under 980 nm excitation, the emission spectra of UCNP@Ag-GOx nanoprobes in the company of glucose solution are shown in Fig. 4A. Notably, increasing glucose concentrations in the range of 0–3.2 μmol L^{-1} leads to the gradual rise of the emission intensity at 540 nm. Additionally, the fluorescence intensity is linearly proportional to the glucose concentration in the scope of 0–3.2 μmol L^{-1}. For the glucose concentration assessment, the calibration function I = 1674C + 2530 with high linearity (R^2 = 0.9953) is established, where I represents the relative emission intensity and C is the glucose concentration (μmol L^{-1}). Thus, the concentration of glucose can be determined by monitoring fluorescence intensity spanning the range of 0–3.2 μmol L^{-1} (Fig. 4B), with the limit of detection (LOD = 3σ/K) computed as 1.77 μmol L^{-1}. The reason why the fluorescence is enhanced is that glucose may be oxidized by O_2 to produce H_2O_2 in the presence of GOx, and then the tiny amount of H_2O_2 can etch Ag layers on the surface of UCNP and convert them into Ag^{+}. Consequently, the decomposition of the Ag layers occurs, which leads to the reversion of the Ag quenching effect accompanied by upconverting emission recovery. Additionally, to further evidence the proposed mechanism, the intermediate H_2O_2 is directly added with the presence of the as-developed sample UCNP@Ag. Likewise, the emission intensity of UCNP@Ag enhanced with the increase of H_2O_2 concentration (Fig. 4C), which implied the interaction occurred between Ag and H_2O_2. In addition, the fluorescence intensity is linearly proportional to the H_2O_2 concentration (Fig. 4D), which is consistent with the results of UCNP@Ag-GOx in glucose solution.

3.5. In vitro selectivity studies

The cytotoxicity of UCNP@Ag-GOx was studied by testing the cell viability in HeLa and MRC-5 cells. As shown in Fig. S6, it was indicated that the nanoprobes were safe for the cells. To further verify the capability of the differentiation between human cervical carcinoma (HeLa) cells and human normal lung fibroblast (MRC-5) cells through interacting with glucose, confocal imaging was performed. HeLa and MRC-5 cell lines were co-incubated with 1 mg mL^{-1} of UCNP and UCNP@Ag-GOx for 24 h. Fluorescence signals in the cells were captured and imaged under 980 nm excitation. As shown in Fig. 5, the signals of UCNP@Ag-GOx in cancer cells were stronger than that of normal cells, whereas there are no diversities between UCNP in HeLa and MRC-5 cells. It is known that cancer cells have a higher uptake rate of glucose than normal cells [41], owing to a greater demand for energy. In HeLa cells, UCNP@Ag-GOx could even recover to a similar fluorescence level with UCNP (Fig. 5A), this is because the higher content of glucose existed in cancer cells over normal cells, GOx on the exterior of the nanoprobes would interact with abundant glucose when the nanoprobes entered the cytoplasm and in turn Ag layer was etched due to the generation of H_2O_2. However, the fluorescence signals of UCNP@Ag-GOx are much lower than UCNP in MRC-5 cells (Fig. 5B) owing to the quenching effect, which is consistent with the experimental results above. Therefore, the discriminatory capability of UCNP@Ag-GOx was evidenced in cancer and normal cells. Further, it is noteworthy that our work is the first study aimed at showcasing the practicality of glucose concentration detection based on lanthanide-doped UCNP. Moreover, this provides a theoretical and experimental basis for the subsequent exploration of the UCNP-based approach to glucose concentration detection.

Lambda scans were run on all the cells and the *in vitro* emission spectra were recorded to observe erbium transitions and verify whether the emission comes from the autofluorescence or the nanoprobe. Typical erbium transitions ($^2H_{11/2} \rightarrow {}^4I_{15/2}$, $^4S_{3/2} \rightarrow {}^4I_{15/2}$, and $^4F_{9/2} \rightarrow {}^4I_{15/2}$) can be observed in the lambda scan under the excitation at 980 nm, as shown in Fig. 5A and B. More importantly, nearly twofold responsive enhancement of upconversion emission was recorded in UCNP@Ag-GOx compared with UCNP in HeLa cells, since the nanoprobe was triggered by high-glucose level in cancer cells to turn on and amplify the upconversion emission of UCNP@Ag-GOx. While there is a threefold drop in UCNP@Ag-GOx compared with UCNP in MRC-5 cells as the quenching effect of UCNP@Ag-GOx has not been recovered. Consequently, it is facile for UCNP@Ag-GOx to distinguish cancer cells from normal cells via optical imaging since a 5-fold emission intensity difference is between them.

4. Conclusions

In conclusion, we presented a sensitive and responsive upconverting fluorescence detection nanoprobe for rapid glucose concentration detection based on an Ag shell modified UCNP core. UCNPs were developed utilizing a facile coprecipitation strategy, and subsequently, Ag layers were built on the surface of the UCNPs. The Ag shells on UCNP's surface function as a quencher. The fluorescence of UCNP was restored by adding glucose after GOx has been anchored on the surface of the UCNP@Ag. In this case, the GOx enables glucose to be oxidized to H_2O_2 (since the nature of GOx is an oxidoreductase), and Ag layers may react immediately with H_2O_2. Consequently, the quenching effect would be rectified in the company of GOx, resulting in Ag layers fragmentation and upconversion emission recovery. Therefore, an efficient and sensitive upconversion fluorescent approach for monitoring glucose concentration can be developed based on detecting enzymatically produced H_2O_2. Notably, the ultralow detection limit of UCNP@Ag-GOx was estimated to be at 1.77 μmol L^{-1}. Furthermore, the upconversion nanoprobe also exhibited extraordinary selectivity over proteins, amino acids, saccharides, and ubiquitous cations. Moreover, the obvious differentiation between cancer cells and normal cells was achieved via confocal imaging. Based on the superior selectivity for glucose and extremely low limit of detection, the upconversion nanoprobes UCNP@Ag-GOx show great prospects in the prevention and early clinical diagnosis of various diseases.

In summary, the as-developed nanoprobe can achieve *in vitro* optical bioimaging in live cells for glucose detection. It is the first report regarding the utilization of lanthanide-based upconverting nanoprobe in biological-related applications with ultrasensitive glucose detection *in vitro*. In addition, the synthesized lanthanide-based upconversion biosensor shows exceptional stability and biocompatibility. The robust biosensing platform possesses ultrahigh sensitivity and capability of on-site and real-time glucose detection *in vitro* and realized a limit of detection (LOD) down to 1.77 μM. Importantly, it is highly expected that the facile-synthesized functional UCNP as a stable and biocompatible nanoplatform has great potential to be expanded to other biomedical fields.

CRediT authorship contribution statement

Shuai Zha: Conceptualization, Methodology, Writing – original draft. **Haolan Li:** Methodology. **Ga-Lai Law:** Methodology. **Ka-Leung Wong:** Resources, Validation, Supervision. **Angelo H. All:** Resources, Validation, Supervision.

Data availability

Data will be made available on request.

Declaration of Competing Interest

The authors declare that they have no known competing financial interests or personal relationships that could have appeared to influence the work reported in this paper.

Acknowledgements

This study was supported by the Hong Kong Baptist University: Start-Up Tier 1 Fund # 21.4531.162640 (PI: A. H. A.), Faculty Seed Fund # 31.4531.179234 (PI: A. H. A.), Initiation Grant for Faculty Niche Research Areas (IG-FNRA) 2020/21 (PI: A. H. A.), Research Grant Council General Research Fund (GRF) 2021-22 (PI: A. H. A.), and NSFC/RGC Joint Research Scheme 2021/2022 N_HKBU209/21(PI: K.-L. W.).

Appendix A. Supplementary material

Supplementary data to this article can be found online at https://doi.org/10.1016/j.matdes.2023.111800.

References

[1] G. Danaei, C.M. Lawes, S. Vander Hoorn, C.J. Murray, M. Ezzati, Global and regional mortality from ischaemic heart disease and stroke attributable to higher-than-optimum blood glucose concentration: comparative risk assessment, Lancet 368 (2006) 1651.
[2] J.A. Morrison, C.J. Glueck, P. Wang, Childhood risk factors predict cardiovascular disease, impaired fasting glucose plus type 2 diabetes mellitus, and high blood pressure 26 years later at a mean age of 38 years: the Princeton-lipid research clinics follow-up study, Metabolism 61 (2012) 531.
[3] D.A. Antonetti, A.J. Barber, S.K. Bronson, W.M. Freeman, T.W. Gardner, L.S. Jefferson, M. Kester, S.R. Kimball, J.K. Krady, K.F. LaNoue, C.C. Norbury, Diabetic retinopathy: seeing beyond glucose-induced microvascular disease, Diabetes 55 (2006) 2401.
[4] L.A. Sechi, C. Catena, L. Zingaro, A. Melis, S. De Marchi, Abnormalities of glucose metabolism in patients with early renal failure, Diabetes 51 (2002) 1226.
[5] J.P. Furet, L.C. Kong, J. Tap, C. Poitou, A. Basdevant, J.L. Bouillot, D. Mariat, G. Corthier, J. Doré, C. Henegar, S. Rizkalla, Differential adaptation of human gut microbiota to bariatric surgery-induced weight loss: links with metabolic and low-grade inflammation markers, Diabetes 59 (2010) 3049.
[6] H.J. Cheon, M.D. Adhikari, M. Chung, T.D. Tran, J. Kim, M.I. Kim, Magnetic nanoparticles-embedded enzyme-inorganic hybrid nanoflowers with enhanced peroxidase-like activity and substrate channeling for glucose biosensing, Adv. Healthc. Mater. 8 (2019) 1801507.
[7] J. Sawayama, S. Takeuchi, Long-term continuous glucose monitoring using a fluorescence-based biocompatible hydrogel glucose sensor, Adv. Healthc. Mater. 10 (2021) 2001286.
[8] J. Cai, W. Luo, J. Pan, G. Li, Y. Pu, L. Si, G. Shi, Y. Shao, H. Ma, J. Guan, Glucose-sensing photonic nanochain probes with color change in seconds, Adv. Sci. 9 (2022) 2105239.
[9] Y.L. Li, Y.H. Liu, L.S. Chen, J.L. Xu, A. Conformable, Gas-permeable, and transparent skin-like micromesh architecture for glucose monitoring, Adv. Healthc. Mater. 10 (2021) 2100046.
[10] J. Zhang, J. Xu, J. Lim, J.K. Nolan, H. Lee, C.H. Lee, Wearable glucose monitoring and implantable drug delivery systems for diabetes management, Adv. Healthc. Mater. 10 (2021) 2100194.
[11] S. Shahrokhian, E.K. Sanati, H. Hosseini, Advanced on-site glucose sensing platform based on a new architecture of free-standing hollow Cu(OH)2 nanotubes decorated with CoNi-LDH nanosheets on graphite screen-printed electrode, Nanoscale 11 (2019) 12655.
[12] W. Lu, M. Jian, Q. Wang, K. Xia, M. Zhang, H. Wang, W. He, H. Lu, Y. Zhang, Hollow core-sheath nanocarbon spheres grown on carbonized silk fabrics for self-supported and nonenzymatic glucose sensing, Nanoscale 11 (2019) 11856.
[13] J. Gu, X. Li, Z. Zhou, W. Liu, K. Li, J. Gao, Y. Zhao, Q. Wang, 2D MnO2 nanosheets generated signal transduction with 0D carbon quantum dots: synthesis strategy, dual-mode behavior and glucose detection, Nanoscale 11 (2019) 13058.
[14] Y. Zhang, S. Li, H. Zhang, H. Xu, Design and application of receptor-targeted fluorescent probes based on small molecular fluorescent dyes, Bioconjug. Chem. 32 (2021) 4–24.
[15] J. Huang, W. Ye, S. Zha, Y. Tao, M. Yang, K. Huang, J. Liu, Y.H. Fung, Y. Li, P. Li, L. Zhu, C.-S. Lee, Sensitive and responsive pentiptycene-based molecular fluorescence chemosensor for detection of polyamines, J. Lumin. 232 (2021) 117856.
[16] R.R. Cheruku, J. Cacaccio, F.A. Durrani, W.A. Tabaczynski, R. Watson, A. Marko, R. Kumar, M.E. El-Khouly, S. Fukuzumi, J.R. Missert, R. Yao, M. Sajjad, D. Chandra, K. Guru, R.K. Pandey, Epidermal growth factor receptor-targeted multifunctional photosensitizers for bladder cancer imaging and photodynamic therapy, J. Med. Chem. 62 (2019) 2598–2617.
[17] G. Bao, S. Zha, Z. Liu, Y.H. Fung, C.F. Chan, H. Li, P.H. Chu, D. Jin, P.A. Tanner, K.-L. Wong, Reversible and sensitive Hg2+ detection by a cell-permeable ytterbium complex, Inorg. Chem. 57 (2018) 120.
[18] J.X. Zhang, M. Pan, C.Y. Su, Synthesis, photophysical properties and in vitro evaluation of a chlorambucil conjugated ruthenium (ii) complex for combined chemo-photodynamic therapy against HeLa cells, J. Mater. Chem. B. 5 (2017) 4623–4632.
[19] H. Li, R. Lan, C.F. Chan, G. Bao, C. Xie, P.H. Chu, W.C. Tai, S. Zha, J.X. Zhang, K.-L. Wong, A luminescent lanthanide approach towards direct visualization of primary cilia in living cells, Chem. Commun. 53 (2017) 7084.
[20] Z. Yi, Z. Luo, X. Qin, Q. Chen, X. Liu, Lanthanide-activated nanoparticles: a toolbox for bioimaging, therapeutics, and neuromodulation, Acc. Chem. Res. 53 (2020) 2692.
[21] K. Du, J. Feng, X. Gao, H. Zhang, Nanocomposites based on lanthanide-doped upconversion nanoparticles: diverse designs and applications, Light Sci. Appl. 11 (2022) 222.
[22] B. Gu, Q. Zhang, Recent advances on functionalized upconversion nanoparticles for detection of small molecules and ions in biosystems, Adv. Sci. 5 (2018) 1700609.
[23] S. Zha, H.F. Chau, W.Y. Chau, L.S. Chan, J. Lin, K.W. Lo, W.C.S. Cho, Y.L. Yip, S.W. Tsao, P.J. Farrell, L. Feng, J.M. Di, G.-L. Law, H.L. Lung, K.-L. Wong, Dual-targeting peptide-guided approach for precision delivery and cancer monitoring by using a safe upconversion nanoplatform, Adv. Sci. 8 (2021) 2002919.
[24] S. Zha, Y.H. Fung, H.F. Chau, J. Lin, J. Wang, L.S. Chan, G. Zhu, H.L. Lung, K.-L. Wong, Responsive upconversion nanoprobe for monitoring and inhibition of EBV-associated cancers via targeting EBNA1, Nanoscale 10 (2018) 15632.
[25] G. Bao, S. Wen, W. Wang, J. Zhou, S. Zha, Y. Liu, K.-L. Wong, D. Jin, Enhancing hybrid upconversion nanosystems via synergistic effects of moiety engineered NIR dyes, Nano Lett. 21 (2021) 9862.
[26] Y. Zhang, X. Ma, H.F. Chau, W. Thor, L. Jiang, S. Zha, W.Y. Fok, H.N. Mak, J. Zhang, J. Cai, C.F. Ng, H. Li, D. Parker, L. Li, G.-L. Law, K.-L. Wong, Lanthanide–cyclen–camptothecin nanocomposites for cancer theranostics guided by near-infrared and magnetic resonance imaging, ACS Appl. Nano Mater. 4 (2021) 271.
[27] S. Zha, K.-L. Wong, A.H. All, Intranasal delivery of functionalized polymeric nanomaterials to the brain, Adv. Healthc. Mater. 11 (2022) 2102610.
[28] S. Zha, F. Yang, Z. Ma, H. Wu, D. Zhang, D. Li, Multifunctional upconversion nanocomposite for multi-purpose cancer theranostics, Mater. Des. 226 (2023) 111682.
[29] Y. Luo, H. Li, M. Cai, Y. Liu, L. Chen, S. Xu, G. Bai, Designing polyacrylic acid capped luminescent rare earth core–shell nanoparticles for simultaneous Cu (II) and temperature sensing, Mater. Des. 224 (2022) 111405.
[30] Z. Su, Y. Zhao, Y. Huang, Y. Lian, S. Xu, G. Bai, Bi-functional nanocomposite based on phosphor and carbon nanotubes for tumor ablation in a photothermal fiber system with temperature feedback, Chem. Eng. J. 436 (2022) 134994.
[31] Y. Liu, G. Bai, Y. Lyu, Y. Hua, R. Ye, J. Zhang, L. Chen, S. Xu, J. Hao, Ultrabroadband tuning and fine structure of emission spectra in lanthanide Er-doped ZnSe nanosheets for display and temperature sensing, ACS Nano 14 (2020) 16003.
[32] J. Yuan, Y. Cen, X.-J. Kong, S. Wu, C.-L. Liu, R.-Q. Yu, X. Chu, MnO2-nanosheet-modified upconversion nanosystem for sensitive turn-on fluorescence detection of H2O2 and glucose in blood, ACS Appl. Mater. Interfaces 7 (2015) 10548–10555.
[33] S. Wu, X.-J. Kong, Y. Cen, J. Yuan, R.-Q. Yu, X. Chu, Fabrication of a LRET-based upconverting hybrid nanocomposite for turn-on sensing of H 2 O 2 and glucose, Nanoscale 8 (2016) 8939–8946.
[34] H. Chen, A. Fang, L. He, Y. Zhang, S. Yao, Sensitive fluorescent detection of H2O2 and glucose in human serum based on inner filter effect of squaric acid-iron(III) on the fluorescence of upconversion nanoparticle, Talanta 164 (2017) 580–587.
[35] H. Li, S. Zha, H. Li, H. Liu, K.-L. Wong, A.H. All, Polymeric dendrimers as nanocarrier vectors for neurotheranostics, Small 18 (2022) 2203629.
[36] M.X. Jiao, A.S. Portniagin, X.L. Luo, L.H. Jing, B.X. Han, A.L. Rogach, Semiconductor nanocrystals emitting in the second near-infrared window: optical properties and application in biomedical imaging, Adv. Opt. Mater. 10 (2022) 2200226.
[37] Z. Li, Z. Gao, C. Wang, D. Zou, H. Zhou, Y. Yi, J. Wang, L. Wang, Recent progress on bioimaging strategies based on Janus nanoparticles, Nanoscale 14 (2022) 12560–12568.
[38] C. Ding, S. Cheng, F. Yuan, C. Zhang, Y. Xian, Ratiometrically pH-insensitive upconversion nanoprobe: toward simultaneously quantifying organellar

calcium and chloride and understanding the interaction of the two ions in lysosome function, Anal. Chem. 94 (2022) 10813–10823.
[39] X. Li, C. Xie, S. Zha, W.S. Tam, M. Jiang, K.-L. Wong, Biocompatible porphyrin-peptide conjugates as theranostic agents targeting the Epstein-Barr virus, ChemPlusChem 87 (2022) e202200184.
[40] F. Jiang, B. Ding, S. Liang, Y. Zhao, Z. Cheng, B. Xing, P. Ma, J. Lin, Intelligent MoS2-CuO heterostructures with multiplexed imaging and remarkably enhanced antitumor efficacy via synergetic photothermal therapy/ chemodynamic therapy/ immunotherapy, Biomaterials 268 (2021) 120545.
[41] L. Chen, H. Li, H. He, H. Wu, Y. Jin, Smart plasmonic glucose nanosensors as generic theranostic agents for targeting-free cancer cell screening and killing, Anal. Chem. 87 (2015) 6868.